Super-resolved Imaging of a Single Cold Atom on a Nanosecond Timescale

Zhong-Hua Qian,[1,2] Jin-Ming Cui,[1,2,*] Xi-Wang Luo,[1,2] Yong-Xiang Zheng,[1,2] Yun-Feng Huang,[1,2,†] Ming-Zhong Ai,[1,2] Ran He,[1,2] Chuan-Feng Li,[1,2,‡] and Guang-Can Guo[1,2]

[1]*CAS Key Laboratory of Quantum Information, University of Science and Technology of China, Hefei, 230026, China*

[2]*CAS Center For Excellence in Quantum Information and Quantum Physics, University of Science and Technology of China, Hefei, 230026, China*

(Received 23 April 2021; revised 3 October 2021; accepted 29 November 2021; published 23 December 2021)

In cold atomic systems, fast and high-resolution microscopy of individual atoms is crucial, since it can provide direct information on the dynamics and correlations of the system. Here, we demonstrate nanosecond-scale two-dimensional stroboscopic pictures of a single trapped ion beyond the optical diffraction limit, by combining the main idea of ground-state depletion microscopy with quantum-state transition control in cold atoms. We achieve a spatial resolution up to 175 nm using a NA $= 0.1$ objective in the experiment, which represents a more than tenfold improvement compared with direct fluorescence imaging. To show the potential of this method, we apply it to observe the secular motion of the trapped ion; we demonstrate a temporal resolution up to 50 ns with a displacement detection sensitivity of 10 nm. Our method provides a powerful tool for probing particle positions, momenta, and correlations, as well as their dynamics in cold atomic systems.

DOI: 10.1103/PhysRevLett.127.263603

Introduction.—Cold atomic systems, including cold quantum gases in optical lattices, neutral atoms in optical tweezers, and trapped ions, are promising platforms to study quantum simulation, computation, and information processing. High-resolution optical detection and imaging of individual particles in these systems are essential procedures, since they can provide direct information on quantum phenomena (e.g., transport, correlations, and phase transitions). In recent decades, many microscope techniques have been developed for cold quantum gases [1,2] and individual atoms in optical tweezers [3,4] or ion traps [5–7]. However, the resolution of these methods is fundamentally restricted to the wavelength scale set by the optical diffraction limit, making them unsuitable for probing quantum phenomena related to the details of the wave function in a variety of many-body systems.

Meanwhile, optical super-resolved microscopy has developed to maturity as a powerful tool in chemistry and biology [8]. It allows chemical reactions and biological processes to be viewed on a nanometer scale [9,10]. In recent years, this method has also been applied to quantum systems, such as imaging of solid-spin systems [11–14] and tracking of single-ion positions [6,15,16], and it has been developed further in combination with quantum techniques for specific systems [17–21]. Realization of detection and manipulation below the subwavelength scale in cold atomic systems would allow the study of quantum transport, correlation, and dynamical phenomena in unprecedented ways, and therefore much research effort has been focused on this area, with substantial progress being made in recent years. Examples include the generation of nanoscale optical potentials [22–24], stroboscopic painting of optical potentials for atoms with subwavelength resolution [25,26], and observation of the wave function of ensembles of atoms in one-dimensional optical lattices based on nonlinear atomic responses [27,28] and pulsed ion microscopy [29]. However, two-dimensional (2D) super-resolved detection of a single cold atom below the optical diffraction limit has yet to be demonstrated.

Here we present a demonstration of ground-state depletion (GSD) microscopy on a trapped ion system to achieve 2D imaging beyond the optical diffraction limit. By combining the control sequence of the GSD microscopy with the qubit states polarization and detection methods for the ion, a 2D image of a trapped ion with a resolution of 175 nm is experimentally realized using a NA $= 0.1$ imaging objective, which is a 13-fold improvement compared with direct fluorescence imaging. Our microscopy method not only enables single-particle imaging of cold atom systems to an unprecedented resolution, but, more importantly, it also has the advantage of high temporal resolution. The depletion process can be very short (around 50 ns) under strong laser power, which enables us to take images in nanosecond intervals and thus allows the measurement of atomic wave function dynamics. To show the capability of our method, we apply it to detect the secular motion of the trapped ion. One cycle of the motion within 735 ns is observed, with a displacement detection sensitivity of 10 nm. Finally, we should point out that our method is quite general and can be applied to both ions and neutral atoms, and it can also be generalized to probe the many-body position correlations and interacting dynamics

of atomic arrays by generating many independent depletion laser spots.

Experiment and results.—The imaging process is based on the transitions between ground states $^2S_{1/2}$ and first excitation states $^2P_{1/2}$ of a $^{171}Yb^+$ ion in a Paul trap (the transition wavelength is 369.5 nm), which are sequentially controlled by different near-resonant lasers. The energy level diagram of $^{171}Yb^+$ is presented in Fig. 1(a). Three different lasers are primarily used for the imaging process: the initialization laser resonates with $^2S_{1/2}|F=1\rangle \leftrightarrow {}^2P_{1/2}|F=1\rangle$, which is used to polarize the nuclear spin states of the ion to $^2S_{1/2}|F=0\rangle$ (dark state); the depletion laser nearly resonates with $^2S_{1/2}|F=0\rangle \leftrightarrow {}^2P_{1/2}|F=1\rangle$, which is used to depopulate the dark state to $^2S_{1/2}|F=1\rangle$ (bright state); the detection laser, with $^2S_{1/2}|F=1\rangle \leftrightarrow {}^2P_{1/2}|F=0\rangle$, is used to detect nuclear spin in a dark or bright state. As the transition between $^2S_{1/2}|F=0\rangle$ and $^2P_{1/2}|F=0\rangle$ is forbidden, the state $S_{1/2}|F=1\rangle$ can

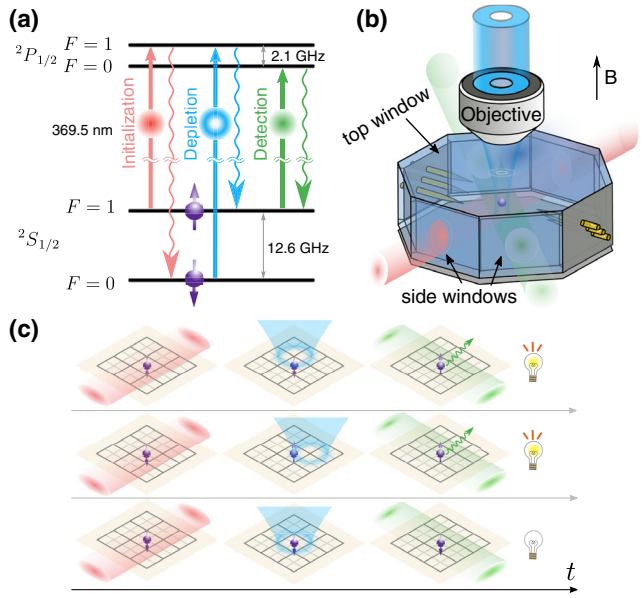

FIG. 1. Experimental scheme and setup. (a) Experimental scheme of energy levels of $^{171}Yb^+$. The ion is optically pumped by a Gaussian beam (red line) and initialized to $^2S_{1/2}|F=0\rangle$ (dark state). Depletion light (blue line) with a doughnut shape pumps the spin into $^2S_{1/2}|F=1\rangle$ (bright state). The detection laser (blue line) is used to read out the ion's state with state-dependent fluorescence. (b) Experimental setup: a Paul trap in a vacuum chamber is used to trap the ion, the initialization beam (red cylinder) and detection beam (green cylinder) are directed from the side windows of the vacuum chamber, and the collimated doughnut beam is focused by the imaging objective (NA = 0.1). (c) Schematic of the super-resolved imaging process, in which three steps in (a) are performed to obtain a pixel of the image. A super-resolved image is obtained by scanning the doughnut spot, and only when the center of the doughnut spot is aligned with the ion does the ion avoid being polarized to the bright state and remains in the dark state.

continually scatter fluorescence photons under the detection laser, which acts as a bright state; by contrast, the state $S_{1/2}|F=0\rangle$ will not scatter detection photons, since it is not resonant with the detection laser, and acts as a dark state [30]. In the depletion process, a doughnut-shaped beam is focused on the ion to polarize its spin state through spontaneous emission. The ion's nuclear spin state is selectively polarized by scanning the doughnut spot position, allowing the position information to be encoded into nuclear spin states. Figure 1(b) shows the configuration of the three lasers in the experimental setup. The $^{171}Yb^+$ ion is trapped in a Paul trap installed in a vacuum chamber [31], and a magnetic field of 9.7 G is applied along the z axis. The initialization laser and detection laser are directed to the trap from the side windows of the chamber. These are Gaussian beams perpendicular to the magnetic field with waists of 30 μm. The depletion light beam is in a doughnut form and, along with the magnetic field, is focused to a doughnut spot through an objective lens with NA = 0.1 and then shone on the trapped ion across the top window of the vacuum chamber.

Figure 1(c) illustrates the main control sequence for the imaging process. The image is obtained pixel by pixel by scanning the depletion spot position on a 2D plane and sequentially switching the three lasers on and off. To illustrate the basic principle of obtaining an image of the ion, here we take just three pixels as an example. Only when the center of the doughnut spot is aligned with the ion does the ion avoid being polarized to the bright state in the depletion process and remains in the dark state. To keep the ion at a low temperature during the imaging process, we apply a 10 MHz red detuned laser containing frequencies of $^2S_{1/2}|F=1\rangle \leftrightarrow {}^2P_{1/2}|F=0\rangle$ and $^2S_{1/2}|F=0\rangle \leftrightarrow {}^2P_{1/2}|F=1\rangle$ for Doppler cooling [32] and switch it on for 1 ms cooling before each pixel imaging sequence [33].

To realize high-spatial-resolution imaging in GSD, a highly focused doughnut spot with high mode purity is crucial, requiring the dark center's residual intensity to be as low as possible. To generate a doughnut spot with high purity, we employ a holographic beam reshaping method with a digital micromirror device (DMD) [42]. Compared with other methods [43–51], we can measure the optical system aberration *in situ* and then compensate for the aberration by this method. Our study first uses the trapped ion as a probe to detect the interference light intensity and measure the aberration phase map of the optical system in combination with the DMD [33]. Subsequently, computer-generated holograph patterns with aberration compensation are calculated and then programmed on the DMD to generate the desired beam profiles. To characterize the quality of focused spots after aberration compensation, we investigate the profiles of reshaped Gaussian and doughnut spots in Laguerre-Gaussian (LG_p^l) modes [LG_0^0 and LG_0^1, see Figs. 2(a) and 2(b), respectively] by scanning the spots around the ion and detecting the ion's fluorescence with a

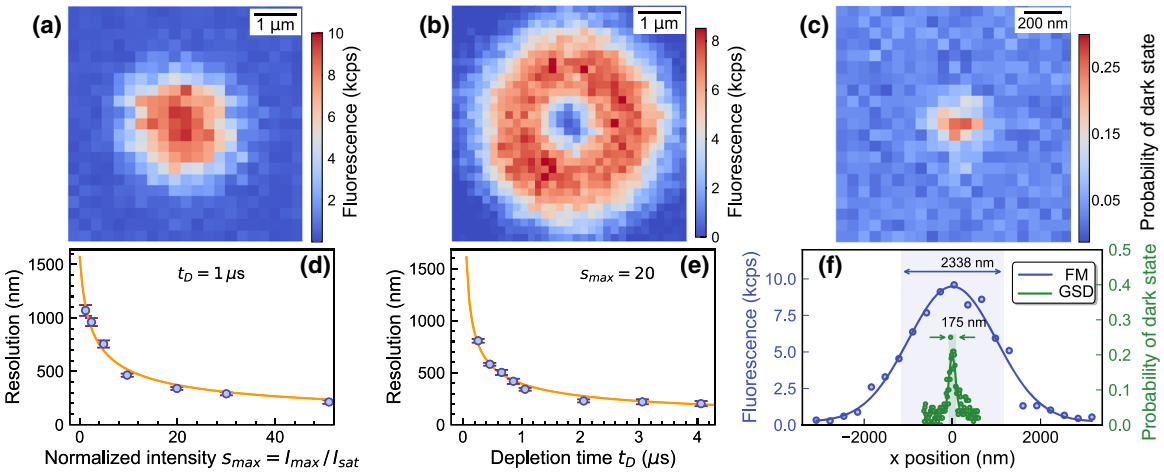

FIG. 2. Demonstration of super-resolved imaging of a trapped ion. (a),(b) Use of the trapped ion as a probe to characterize the profile of Gaussian and doughnut spots, respectively, after aberration compensation using DMD with the holographic beam reshaping method [42]. The intensity is represented by the number of scattered fluorescence photons measured per second (kilocounts per second, kcps). The minimum intensity of the doughnut spot in the center is 3.8% of the maximum intensity. (c) Super-resolved image of a single ion. The depletion laser is linearly polarized, and the probability of the dark state is obtained from the statistics of 100 measurements. (d) Spatial resolution (FWHM) as a function of normalized intensity $s_{\max} = I_{\max}/I_{\text{sat}}$ of doughnut light for 1 μs depletion time. (e) Spatial resolution as a function of depletion time with $s_{\max}$ fixed at 20. (f) Contrast of resolutions between fluorescence microscope (FM) and GSD microscope with depletion time $t_D = 7$ μs and depletion power $P = 65$ nW ($s_{\max} = 14$). The solid lines are fits with Gaussian functions.

cooling laser. The Gaussian spot is focused to a full width at half maximum (FWHM) of 2.34 μm, which is at its diffraction limit. For the doughnut beam, the residual light intensity in the dark center is 3.8% of the maximum intensity.

After preparation of the dark-center doughnut spot, the imaging sequences in Fig. 1(c) were applied with a linearly polarized doughnut beam. A super-resolved image of a single trapped ion was obtained, as shown in Fig. 2(c). The FWHM in the x axis is 175 nm at 65 nW depletion laser power and 7 μs depletion time. A comparison of the measured point spread functions, shown in Fig. 2(f), reveals that this technique gives a 13-fold improvement in spatial resolution over fluorescence microscopy. We also analyzed the resolution as a function of the intensity and pulse duration of the depletion light, and the results are shown in Figs. 2(d) and 2(e). Here, for generality, the intensity is characterized by the normalized intensity $s_{\max} = I_{\max}/I_{\text{sat}}$, where $I_{\max}$ denotes the maximum intensity of the doughnut spot profile and $I_{\text{sat}} = 510$ W/m^2 is the saturation intensity of the Yb^+ ion. The results are consistent with the spatial resolution Δr of the simplified model [33],

$$\Delta r = \frac{\mathcal{W}_{01}}{\sqrt{1 + k s_{\max} t_D}} = \frac{\mathcal{W}_{00}}{1.67\sqrt{1 + k s_{\max} t_D}}, \qquad (1)$$

where the coefficient $k = \beta\sigma I_{\text{sat}}/\hbar\omega_0$, $ks_{\max}$ represents the depletion rate, $\mathcal{W}_{01} = 1.41$ μm is the FWHM of the central hollow area of the doughnut spot (LG_0^1 mode), $\mathcal{W}_{00} = 2.34$ μm is the FWHM of the Gaussian spot (LG_0^0 mode), β is the branching ratio for the decay into the bright state, σ is the cross section [52], and t_D is the depletion pulse duration. This model indicates that the resolution is determined by the product of $s_{\max}$ and t_D. Theoretically, the resolution can be extended to the sub-nanometer scale as long as we increase $s_{\max} t_D$. However, further improvement in resolution is limited by actual experiment conditions. First, the imperfection of the doughnut spot results in residual light in the center. As the doughnut power increases, the residual light in the center s_0 will be large enough to excite the spin and make the position information indistinguishable from the probability noise. The resolution limit [33] $\Delta r_{\text{limit}} \propto \lambda/(\text{NA}\sqrt{E})$, where $E = I_{\max}/I_0$ is defined as the extinction ratio of the doughnut spot. Second, the spatial resolution is limited by the ion's wave packet size after cooling, which is about 20 nm, as given by the Doppler cooling limit in the present study.

Next, we will present a method to detect the dynamics of a single cold atom in a 2D plane with high precision. Because the ion is trapped in a harmonic trap, it undergoes secular oscillations in three axes [53]. Here, we select the oscillation along two rf needles (the y axis) for the study, as shown in Fig. 3(a). To demonstrate this application, we first drive the ion resonantly with an electrical pulse to excite the oscillation along the y axis after Doppler cooling. The electrical pulse provides a driving force in the form $F_d \sin(\omega_d t)$, which drives at a frequency ω_d and lasts for a time t_d. During the driving process, the cooling lasers are turned off to avoid motion dissipation. When the driving

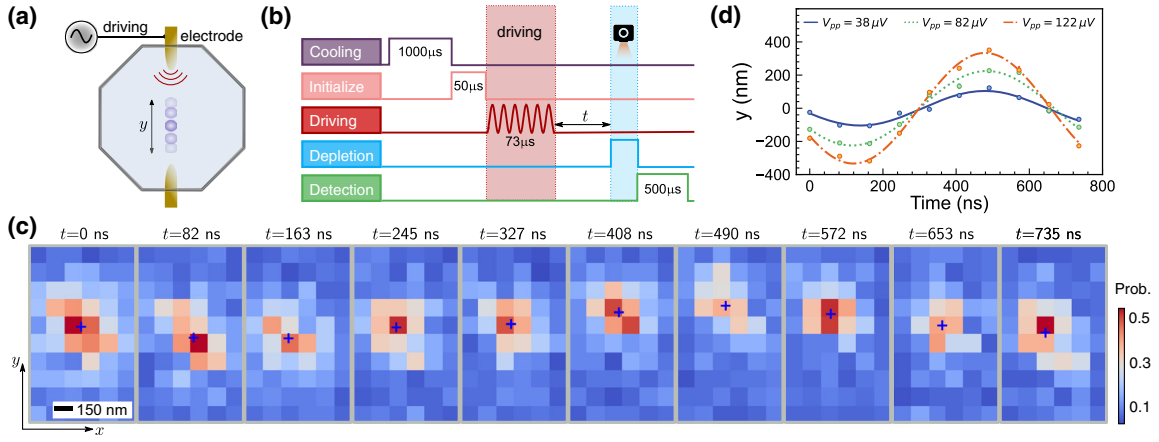

FIG. 3. Nanosecond photography to detect the dynamics of the trapped ion. (a) To excite the motion mode along the y axis, a resonant electrical signal is applied to one electrode of the Paul trap, providing a sinusoidal driving force. (b) Sequence diagram of the imaging process. The ion is driven to steady oscillation by a resonant pulse, with a driving voltage V_{pp} and a driving duration of 73.5 μs. The ion is then imaged at t after the driving has been stopped, with a 50 ns depletion duration. s_{max} is fixed at 450. (c) Photographs of the moving ion driven by $V_{\mathrm{pp}} = 38$ μV at different t. The blue crosses mark the fitted centers. (d) The ion's motional trajectories along the y axis under different driving voltages, which are constructed by the fitted centers of super-resolved images.

pulse ends, the ion is driven into a steady-state oscillation, and the amplitude of the oscillation is given by

$$A = \frac{2F_d}{m(\omega_y^2 - \omega_d^2)} \sin\left[\frac{(\omega_y - \omega_d)t_d}{2}\right], \tag{2}$$

where $\omega_y = 2\pi \times 1.36$ MHz is the oscillation frequency of the ion, $t_d = 100T = 100 \times 2\pi/\omega_y$, and m is the ion mass. Near resonance $(\omega_d \approx \omega_y)$, we find that $A = F_d t_d / 2m\omega_y$, which indicates that the amplitude of motion is proportional to the driving force F_d and driving time t_d.

To acquire the instantaneous position of the ion at time t after the driving pulse, we implement the super-resolved microscopy with a delay time t before the depletion process. To get a pixel in an image, a control sequence in Fig. 3(b) is repeated 100 times to get the dark-state probability, which requires 0.16 s. As the excited oscillation is synchronized to the driving wave phase, we fix the driving wave phase to make sure the current position of the ion is constant between different shots. To obtain one image, the doughnut beam is scanned to 10×10 pixels, while the depletion pulse duration is kept at 50 ns, which is much shorter than the period of motion (735 ns). The normalized intensity of the doughnut spot s_{max} is fixed at 450. The total time to get an image is 16 s. By imaging the ion at different t, we can see its dynamics in the trap. Figure 3(c) shows a typical photographic recording of the oscillating ion in the central 6×10 pixels. By fitting each image to obtain the displacements of the ion at different t, the ion trajectory can be reconstructed with a precision of 10 nm. The fitted spatial resolution is averaged as 373 nm. The ion's oscillating trajectories under different driving forces are also investigated in this study, as shown in Fig. 3(d). The result shows that the amplitude of motion depends linearly on the driving force, as predicted by Eq. (2). We observed an amplitude of motion of 104.2 ± 8.9 nm under a 38 μV peak-to-peak driving voltage ($V_{\mathrm{pp}} = 38$ μV). The corresponding driving force $F_d = 6.9 \pm 0.7$ zN. The period of motion is fitted as 681.1 ± 23.9 ns, which has a 7% error relative to the calculated period.

Outlook and conclusions.—In this Letter, we have demonstrated a nanosecond-scale super-resolved 2D imaging method for a single trapped ion. Our approach is quite general and can be applied to both charged atoms (e.g., the trapped ion studied here) and neutral ultracold atoms (e.g., a single atom trapped in an optical tweezer), for which the holographic beam reshaping method with DMD [42] as well as (nuclear-) spin polarization and detection have already been widely used. Moreover, an arbitrary array of spots with various shapes can be easily generated at the same time, using the holographic beam reshaping method [42], and each of them can be controlled independently. Therefore, by applying these depletion spots in parallel on site-resolved cold atoms (e.g., tweezer arrays), we can develop this imaging method to probe two- or multisite correlations and their interacting many-body dynamics.

It is worth noting that the resolution of the microscopy can be improved by using higher-NA objectives under the same depletion parameters (e.g., the NAs of objectives have reached 0.6 for trapped ion systems [6] and 0.7 for cold neutral atoms in optical tweezers [3]), and the GSD schemes will support an imaging resolution below 30 nm and a displacement measurement accuracy below 2 nm, in principle, which is below the level of the wave packet size

of the motional ground state. Furthermore, the limit of resolution is approximately $\mathcal{W}_{01}/\sqrt{-E\ln\Delta p}$ [33]; by reducing the E [42,49,54] and improving the detection fidelity of the dark state Δp [55], the resolution can further reach 3.1 nm under an objective with NA = 0.6.

Together with the advantage of nanosecond imaging time, our work opens up new opportunities in the study of single-particle dynamics, many-body correlation [56], and even two-body collision dynamics [57] in cold atomic systems. For example, long-range interactions based on Rydberg atoms and ions could induce two-particle entanglement in position and momentum even when they are far apart (with site addressability), and applying fast and high-resolution imaging of each particle allows direct measurement of both two-particle position correlation and particle dynamics, with no need for any additional mapping or time-of-flight operation [56]. Our method can even be used to measure short-range correlations with contact interactions (e.g., the spin-exchange interaction [3,56]), as long as the two interacting atoms are distinguishable particles (e.g., different species or spins). We can first coherently transfer a spin-up (or spin-down) state from the S to the D level to store the spin, and then apply the GSD sequence to measure the position of the spin-down (or spin-up) state, while using different wavelengths to image different species.

In conclusion, we have presented a nanosecond-scale super-resolved imaging method to detect a single trapped ion and its dynamics in two dimensions, achieving a spatial-time resolution to 175 nm at 7 μs and 373 nm at 50 ns, and the resolution can be improved further using higher-NA objectives. The method is general and can be used for both charged and neutral cold atoms. It can also be developed further to detect many-body correlations using multiple GSD spots. Furthermore, the GSD method on a cold atom system can be extended in the future to three dimensions, like classical GSD [12], thereby further enhancing its potential.

This work was supported by the National Key Research and Development Program of China (Grants No. 2017YFA0304100 and No. 2016YFA0302700), the National Natural Science Foundation of China (Grants No. 11821404, No. 11874343, No. 11774335, and No. 11734015), the Key Research Program of Frontier Sciences, CAS (Grant No. QYZDY-SSW-SLH003), the Science Foundation of the CAS (Grant No. ZDRW-XH-2019-1), the Fundamental Research Funds for the Central Universities (Grants No. WK2470000026, No. WK2470000027, and No. WK2470000028), the Anhui Initiative in Quantum Information Technologies (Grants No. AHY020100 and No. AHY070000), and the National Program for Support of Topnotch Young Professionals (Grant No. BB2470000005).

Z.-H. Q. and J.-M. C. contributed equally to this work.

Note added.—Recently, we became aware of recent work on optical super-resolution sensing of a trapped ion's wave packet size [58], which uses the ground-state depletion technique to detect the size of the motion wave packet of a trapped Ca^+ ion.

*jmcui@ustc.edu.cn
†hyf@ustc.edu.cn
‡cfli@ustc.edu.cn

[1] W. S. Bakr, J. I. Gillen, A. Peng, S. Fölling, and M. Greiner, Nature (London) **462**, 74 (2009).
[2] E. Haller, J. Hudson, A. Kelly, D. A. Cotta, B. Peaudecerf, G. D. Bruce, and S. Kuhr, Nat. Phys. **11**, 738 (2015).
[3] A. M. Kaufman, B. J. Lester, M. Foss-Feig, M. L. Wall, A. M. Rey, and C. A. Regal, Nature (London) **527**, 208 (2015).
[4] H. Levine, A. Keesling, G. Semeghini, A. Omran, T. T. Wang, S. Ebadi, H. Bernien, M. Greiner, V. Vuletić, H. Pichler, and M. D. Lukin, Phys. Rev. Lett. **123**, 170503 (2019).
[5] H. Nägerl, D. Leibfried, F. Schmidt-Kaler, J. Eschner, and R. Blatt, Opt. Express **3**, 89 (1998).
[6] J. D. Wong-Campos, K. G. Johnson, B. Neyenhuis, J. Mizrahi, and C. Monroe, Nat. Photonics **10**, 606 (2016).
[7] L. A. Zhukas, M. J. Millican, P. Svihra, A. Nomerotski, and B. B. Blinov, Phys. Rev. A **103**, 023105 (2021).
[8] B. O. Leung and K. C. Chou, Appl. Spectrosc. **65**, 967 (2011).
[9] R. F. Hamans, M. Parente, and A. Baldi, Nano Lett. **21**, 2149 (2021).
[10] M. Sunbul, J. Lackner, A. Martin, D. Englert, B. Hacene, F. Grün, K. Nienhaus, G. U. Nienhaus, and A. Jäschke, Nat. Biotechnol., **39**, 686 (2021).
[11] E. Rittweger, K. Y. Han, S. E. Irvine, C. Eggeling, and S. W. Hell, Nat. Photonics **3**, 144 (2009).
[12] K. Y. Han, K. I. Willig, E. Rittweger, F. Jelezko, C. Eggeling, and S. W. Hell, Nano Lett. **9**, 3323 (2009).
[13] P. C. Maurer, J. R. Maze, P. L. Stanwix, L. Jiang, A. V. Gorshkov, A. A. Zibrov, B. Harke, J. S. Hodges, A. S. Zibrov, A. Yacoby, D. Twitchen, S. W. Hell, R. L. Walsworth, and M. D. Lukin, Nat. Phys. **6**, 912 (2010).
[14] R. Kolesov, S. Lasse, C. Rothfuchs, A. D. Wieck, K. Xia, T. Kornher, and J. Wrachtrup, Phys. Rev. Lett. **120**, 033903 (2018).
[15] M. J. Biercuk, H. Uys, J. W. Britton, A. P. VanDevender, and J. J. Bollinger, Nat. Nanotechnol. **5**, 646 (2010).
[16] V. Blums, M. Piotrowski, M. I. Hussain, B. G. Norton, S. C. Connell, S. Gensemer, M. Lobino, and E. W. Streed, Sci. Adv. **4**, eaao4453 (2018).
[17] D. D. Yavuz and N. A. Proite, Phys. Rev. A **76**, 041802(R) (2007).
[18] A. V. Gorshkov, L. Jiang, M. Greiner, P. Zoller, and M. D. Lukin, Phys. Rev. Lett. **100**, 093005 (2008).
[19] J.-M. Cui, F.-W. Sun, X.-D. Chen, Z.-J. Gong, and G.-C. Guo, Phys. Rev. Lett. **110**, 153901 (2013).
[20] R. Tenne, U. Rossman, B. Rephael, Y. Israel, A. Krupinski-Ptaszek, R. Lapkiewicz, Y. Silberberg, and D. Oron, Nat. Photonics **13**, 116 (2019).

[21] D. Yang, C. Laflamme, D. V. Vasilyev, M. A. Baranov, and P. Zoller, Phys. Rev. Lett. **120**, 133601 (2018).
[22] M. Lacki, M. A. Baranov, H. Pichler, and P. Zoller, Phys. Rev. Lett. **117**, 233001 (2016).
[23] Y. Wang, S. Subhankar, P. Bienias, M. Lacki, T.-C. Tsui, M. A. Baranov, A. V. Gorshkov, P. Zoller, J. V. Porto, and S. L. Rolston, Phys. Rev. Lett. **120**, 083601 (2018).
[24] W. Ge and M. S. Zubairy, Phys. Rev. A **101**, 023403 (2020).
[25] M. Lacki, P. Zoller, and M. A. Baranov, Phys. Rev. A **100**, 033610 (2019).
[26] T.-C. Tsui, Y. Wang, S. Subhankar, J. V. Porto, and S. L. Rolston, Phys. Rev. A **101**, 041603(R) (2020).
[27] M. McDonald, J. Trisnadi, K.-X. Yao, and C. Chin, Phys. Rev. X **9**, 021001 (2019).
[28] S. Subhankar, Y. Wang, T.-C. Tsui, S. L. Rolston, and J. V. Porto, Phys. Rev. X **9**, 021002 (2019).
[29] C. Veit, N. Zuber, O. A. Herrera-Sancho, V. S. V. Anasuri, T. Schmid, F. Meinert, R. Löw, and T. Pfau, Phys. Rev. X **11**, 011036 (2021).
[30] B. B. Blinov, D. Leibfried, C. Monroe, and D. J. Wineland, Quantum Inf. Process. **3**, 45 (2004).
[31] Z. Wang, L. Luo, K. Thadasina, K. Qian, J. Cui, and Y. Huang, EPJ Tech. Instrum. **3**, 3 (2016).
[32] S. Olmschenk, K. C. Younge, D. L. Moehring, D. N. Matsukevich, P. Maunz, and C. Monroe, Phys. Rev. A **76**, 052314 (2007).
[33] See Supplemental Material at http://link.aps.org/supplemental/10.1103/PhysRevLett.127.263603 for details of the laser system (Sec. II), details of holographic beam reshaping with DMD (Sec. III), and derivation of limits (Sec. VIII), which includes Refs. [34–41].
[34] E. D. Black, Am. J. Phys. **69**, 79 (2001).
[35] C.-Y. Shih, S. Motlakunta, N. Kotibhaskar, M. Sajjan, R. Hablützel, and R. Islam, npj Quantum Inf. **7**, 57 (2021).
[36] Y. Liu, Q. Zhang, and X. Su, Opt. Lasers Eng. **74**, 22 (2015).
[37] J. Novák, P. Novák, and A. Mikš, Opt. Commun. **281**, 5302 (2008).
[38] W.-H. Lee, Appl. Opt. **18**, 3661 (1979).
[39] K. G. Johnson, J. D. Wong-Campos, A. Restelli, K. A. Landsman, B. Neyenhuis, J. Mizrahi, and C. Monroe, Rev. Sci. Instrum. **87**, 053110 (2016).
[40] J. R. Johansson, P. D. Nation, and F. Nori, Comput. Phys. Commun. **184**, 1234 (2013).
[41] V. Westphal and S. W. Hell, Phys. Rev. Lett. **94**, 143903 (2005).
[42] P. Zupancic, P. M. Preiss, R. Ma, A. Lukin, M. E. Tai, M. Rispoli, R. Islam, and M. Greiner, Opt. Express **24**, 13881 (2016).
[43] M. Beijersbergen, R. Coerwinkel, M. Kristensen, and J. Woerdman, Opt. Commun. **112**, 321 (1994).
[44] S. S. R. Oemrawsingh, J. A. W. van Houwelingen, E. R. Eliel, J. P. Woerdman, E. J. K. Verstegen, J. G. Kloosterboer, and G. W. 't Hooft, Appl. Opt. **43**, 688 (2004).
[45] M. Beijersbergen, L. Allen, H. van der Veen, and J. Woerdman, Opt. Commun. **96**, 123 (1993).
[46] D. V. Petrov, F. Canal, and L. Torner, Opt. Commun. **143**, 265 (1997).
[47] S. Slussarenko, A. Murauski, T. Du, V. Chigrinov, L. Marrucci, and E. Santamato, Opt. Express **19**, 4085 (2011).
[48] V. D'Ambrosio, N. Spagnolo, L. D. Re, S. Slussarenko, Y. Li, L. C. Kwek, L. Marrucci, S. P. Walborn, L. Aolita, and F. Sciarrino, Nat. Commun. **4**, 2432 (2013).
[49] L. Yan, P. Gregg, E. Karimi, A. Rubano, L. Marrucci, R. Boyd, and S. Ramachandran, Optica **2**, 900 (2015).
[50] Y. Fang-Wei and L. Yong-Ping, Acta Phys. Sinica **52**, 328 (2003).
[51] Q. Xiao-Qing, G. Chun-Qing, and L. Yi-Dong, Acta Phys. Sinica **59**, 264 (2010).
[52] C. Foot, *Atomic Physics* (Oxford University Press, Oxford, 2005).
[53] D. Leibfried, R. Blatt, C. Monroe, and D. Wineland, Rev. Mod. Phys. **75**, 281 (2003).
[54] L. Yan, P. Kristensen, and S. Ramachandran, APL Photonics **4**, 022903 (2019).
[55] R. Noek, G. Vrijsen, D. Gaultney, E. Mount, T. Kim, P. Maunz, and J. Kim, Opt. Lett. **38**, 4735 (2013).
[56] A. Bergschneider, V. M. Klinkhamer, J. H. Becher, R. Klemt, L. Palm, G. Zürn, S. Jochim, and P. M. Preiss, Nat. Phys. **15**, 640 (2019).
[57] Q. Guan, V. Klinkhamer, R. Klemt, J. H. Becher, A. Bergschneider, P. M. Preiss, S. Jochim, and D. Blume, Phys. Rev. Lett. **122**, 083401 (2019).
[58] M. Drechsler, S. Wolf, C. T. Schmiegelow, and F. Schmidt-Kaler, Phys. Rev. Lett. **127**, 143602 (2021).